Enabling Alternative Ethylene Production through Its Selective Adsorption in the Metal–Organic Framework Mn2(m-dobdc)

Journal:	*Energy & Environmental Science*
Manuscript ID	EE-ART-05-2018-001332.R1
Article Type:	Paper
Date Submitted by the Author:	08-Jun-2018
Complete List of Authors:	Bachman, Jonathan; Stanford University, Materials Science & Engineering Reed, Douglas; University of California, Berkeley, Chemistry Kapelewski, Matthew; University of California Berkeley, Chemistry ; E O Lawrence Berkeley National Laboratory, Chachra, Gaurav; Siluria Technologies Jonnavittula, Divya; Siluria Technologies Radaelli, Guido; Siluria Technologies Long, Jeffrey; University of California, Berkeley, Department of Chemistry

Energy & Environmental Science

ARTICLE

Enabling Alternative Ethylene Production through Its Selective Adsorption in the Metal–Organic Framework Mn_2(*m*-dobdc)

Received 00th January 20xx,
Accepted 00th January 20xx

DOI: 10.1039/x0xx00000x

www.rsc.org/

Jonathan E. Bachman,[a,b] Douglas A. Reed,[a] Matthew T. Kapelewski,[a] Gaurav Chachra,[c] Divya Jonnavittula,[c] Guido Radaelli,[c] and Jeffrey R. Long[a,d,e*]

The unique adsorptive properties of metal–organic frameworks open the door to new processes for energy and raw materials production. One such process is the oxidative coupling of methane for the generation of ethylene, which has limited viability due to the high cost of cryogenic distillation. Rather than employing such a traditional separation route, we propose the use of a porous material that is highly selective for ethylene over a wide range of gases in an energy- and cost-effective adsorbent-based separation process. Here, we analyze the metal–organic frameworks M_2(*m*-dobdc) (M = Mg, Mn, Fe, Co, Ni; *m*-dobdc^{4-} = 4,6-dioxido-1,3-benzenedicarboxylate), featuring a high density of coordinatively-unsaturated M^{2+} sites, along with the commerial adsorbent zeolite CaX, for their ability to purify ethylene from the effluent of an oxidative coupling of methane process. Our results show that unique metal–adsorbate interactions facilitated by Mn_2(*m*-dobdc) render this material an outstanding adsorbent for the capture of ethylene from the product mixture, enabling this potentially disruptive alternative process for ethylene production.

Broader Context
Ethylene is a ubiquitous feedstock in the petrochemical industry and is primarily derived from naphtha or ethane cracking. A potentially more renewable approach to its generation involves the catalytic conversion of methane via an oxidative coupling mechanism, but this reaction produces ethylene amongst a broad mixture of gases, including mainly H_2, CH_4, C_2H_6, CO, and CO_2. Currently, the low methane conversion and modest ethylene selectivity of the reaction necessitate the use of costly cryogenic separations to produce high-purity ethylene. Instead, adsorption could ideally provide a method to selectively separate ethylene from this gas mixture without the need for cryogenic separations. However, no adsorbent has been shown to demonstrate sufficient selectivity for ethylene from this gas mixture. The development of the metal–organic frameworks presented here enables the oxidative-coupling of methane process via a low-cost separation route.

Introduction

The pursuit of renewable raw materials and processes for the production of global commodity chemicals is a challenging yet critical enterprise toward a more sustainable energy future, alongside a transition away from fossil fuels to renewable energy sources. Ethylene is one ubiquitous raw material that is currently produced on massive scales—exceeding 150 million tonnes/year—and is primarily derived from cracking of naphtha and ethane.[1] In considering alternative routes to ethylene that do not rely on these fossil resources, significant attention has been given to the oxidative coupling of methane (OCM)[2-15] and the conversion of methanol-to-olefins (MTO).[16-21] Methanol itself is commonly derived from syngas generated by coal gasification or other petrochemical routes and therefore it is not an efficient precursor to renewable ethylene. Alternatively, the OCM process uses methane as a feedstock for ethylene production. Methane is an important intermediary as both an energy carrier and feedstock in the transition away from a fossil fuel-based economy to one primarily supplied through alternative energy; and with the advent of hydraulic fracturing, the displacement of coal with natural gas has been the primary driver for reduced CO_2 emissions in the United States in recent years.[22] Further, methane can be produced through a variety of renewable means, such as from biomass sources including agricultural waste,[23] wastewater,[24] landfills,[25] or via electrochemical CO_2 reduction.[26] Using methane to replace

[a] Department of Chemistry, University of California, Berkeley, Berkeley CA 94720.
[b] Department of Materials Science and Engineering, Stanford University, Stanford CA 94305.
[c] Siluria Technologies Inc., 409 Illinois St., San Francisco CA 94158.
[d] Materials Sciences Division, Lawrence Berkeley National Laboratory, Berkeley CA 94720.
[e] Department of Chemical and Biomolecular Engineering, University of California, Berkeley, Berkeley CA 94720.
Electronic Supplementary Information (ESI) available:
See DOI: 10.1039/x0xx00000x

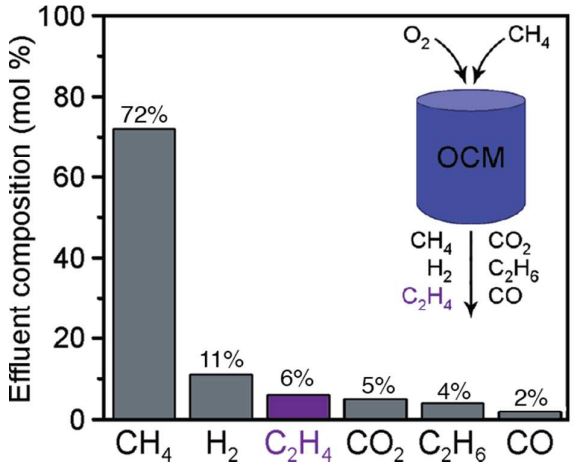

Fig. 1 Block-flow schematic illustrating oxidative coupling of methane (OCM) and effluent composition. The reactants O_2 and CH_4 are fed into the OCM reactor and undergo coupling and cracking reactions to produce an effluent stream comprising CH_4, H_2, C_2H_4, CO_2, C_2H_6, CO, and other minor impurities.

Table 1 Physical and thermodynamic parameters of the primary small molecules composing the effluent in the oxidative coupling of methane, including the kinetic diameter, boiling point, dipole moment (μ), quadrupole moment (Θ), and polarizability (α).

	Kinetic Diameter (Å)	Boiling Point (K)	μ (10^{30} C·M)	Θ (10^{-40} C·m^2)	α (10^{-25} cm^3)
CH_4	3.758	111	0	0	25.93
H_2	2.89	20.3	0	2.21	8.042
C_2H_4	4.163	169.4	0	5.00	42.52
CO_2	3.300	216.55	0	14.33	29.11
C_2H_6	4.444	184.5	0	2.17	44.7
CO	3.690	81.66	0.329	8.33	19.5

petroleum sources as a raw material for the production of ethylene would also ease a transition from fossil fuels to a more sustainable economy.

Large-scale implementation of OCM currently has limited viability, however, because methane–to–ethylene conversion is low and ethylene is generated together with several other products, including ethane, CO_2, CO, and H_2 (Fig. 1). It is difficult to separate these components through a conventional scrubbing and distillation cascade, in which a high volume of methane and other products would need to be recycled in order to maximize carbon efficiency. Additionally, the OCM catalyst and reactor conditions dictate product stream composition, such that it is challenging to adopt a general solution to this separation. Finally, the OCM purification process is associated with high energy and capital costs that often make it infeasible in practice.

One avenue to address this separations challenge is through the use of an adsorbent that can selectively capture ethylene over the other OCM product stream components, eliminating the need for multiple separation operations in series. Upon inspection of the kinetic diameter, boiling point, dipole moment, quadrupole moment, and polarizability for each gas, it is clear, however, that ethylene has no single physical or thermodynamic property that can be used as a handle to separate it from this complex mixture in a single unit operation using traditional distillation or conventional adsorbents (Table 1).

Alternatively, we considered that metal–organic frameworks—a class of permanently porous, highly-tunable adsorbents—could offer an intriguing solution to this separations challenge. Consisting of metal nodes connected by organic linkers,[27-36] metal–organic frameworks have been studied extensively and found to show great promise for various CO_2 and hydrocarbon gas separations.[37–53] However, the separation of any one component from a complex mixture of molecules exhibiting similar physicochemical properties, as is needed here, requires a level of selectivity that has not yet been demonstrated. Certain techniques have been devised that facilitate selective adsorption of a single component over a variety of species; however, these methods typically require the target adsorbate to possess a chemical or physical handle—such as the Lewis acidity of CO_2 or the distinct sizes and shapes of different hydrocarbons—that differentiates it from the other molecules and facilitates tailored framework design.[54-56] Because ethylene lacks such distinguishing handles relative to the other gases in the OCM product mixture, we sought to utilize a framework with open metal sites, pursuing an approach that involves balancing the electropositivity and π-backbonding ability of the coordinating metal site for achieving selectivity.

In choosing a suitable framework, it was of paramount importance to find a material capable of selectively adsorbing ethylene from the given mixture. Furthermore, given the substantial amounts of adsorbent required in an industrial process, we sought a material with a high capacity for ethylene that could in part offset the associated materials costs. An ideal material would also undergo rapid adsorption and facile regeneration, allowing the ethylene to be collected and the material bed regenerated without the need for large swings in temperature or pressure. Finally, we sought a material that could be produced on large scales without prohibitive cost. Along these lines, we recently reported that the framework Fe_2(*m*-dobdc) (*m*-dobdc^{4-} = 4,6-dioxido-1,3-benzenedicarboxylate) is a promising candidate adsorbent for ethylene/ethane and propylene/propane separations.[53] This material exhibits 11 Å-wide channels lined with a high concentration of Fe^{2+} ions, each featuring a single open coordination site that can selectively bind ethylene, resulting in a high ethylene uptake capacity and fast adsorption kinetics. In the context of this study, we identified the M_2(*m*-dobdc) family of frameworks (M = Mg, Mn, Fe, Co, and Ni) as promising candidates meeting the above design criteria, with advantages including reasonable regeneration conditions and

low production costs that render them particularly attractive materials for commercial applications. Most importantly, framework–guest interactions can be finely tuned by varying the metal center, governing metal–ethylene, –ethane, $–CO_2$, and –CO interactions.

Here, we characterize the ability of M_2(*m*-dobdc) (M = Mg, Mn, Fe, Co, Ni) framework materials to selectively adsorb ethylene in a model OCM product stream, and compare this data to that obtained for zeolite CaX, which is commercially used for CO_2 separations and has also been shown to selectively adsorb ethylene over ethane.[57,58] Further, experimental breakthrough data obtained on these materials are compared to results obtained for a simulated separation of an OCM product mixture. Our results demonstrate that the M_2(*m*-dobdc) materials are generally superior to CaX in the separation of ethylene from the OCM mixture, with Mn_2(*m*-dobdc) displaying an electronic structure that is most conducive to the selective adsorption of ethylene.

Experimental

The M_2(*m*-dobdc) (M = Mg, Mn, Fe, Co, Ni) materials were synthesized and prepared for adsorption experiments according to previously reported methods.[53,59] Zeolite CaX was purchased from Tosoh Corporation in the form of 1.5-mm spherical pellets with 9 Å pores and was activated at 180 ˚C under dynamic vacuum in a pre-weighed sample tube. Its activated mass was recorded as a basis for adsorption experiments.

Single-component equilibrium adsorption isotherms

Single-component equilibrium gas adsorption data were collected at pressures ranging from 0 to 1.1 bar using a Micromeritics 3Flex instrument, which employs a volumetric method to determine the amount of gas adsorbed at equilibrium pressure. Activated samples were transferred under a dry N_2 atmosphere into pre-weighed sample tubes and capped with a Micromeritics Transeal. Samples were then evacuated at 180 °C under a dynamic vacuum (<10^{-5} bar), until the off-gas rate was <10^{-7} bar/s. The evacuated tubes and samples were then weighed to determine the mass of the activated sample, typically 30–100 mg. The free-space of each sample was then measured using UHP He (99.999%) prior to adsorption isotherm collection. Gas adsorption isotherm data for ethylene, ethane, CO, CO_2, and CH_4 were collected at 25, 35, and 45 °C, using a water circulator for temperature control. Between each isotherm measurement, samples were reactivated by heating at 180 °C under dynamic vacuum for at least 2 h. Oil-free vacuum pumps and oil-free pressure regulators were used for all sample preparations and measurements.

Isotherm Fitting

The single-component gas adsorption isotherms were fit using a dual-site Langmuir–Freundlich equation, given by eqn 1:

$$n = \frac{q_{\mathrm{sat,a}} b_{\mathrm{a}} P^{\nu_{\mathrm{a}}}}{1+b_{\mathrm{a}} P^{\nu_{\mathrm{a}}}} + \frac{q_{\mathrm{sat,b}} b_{\mathrm{b}} P^{\nu_{\mathrm{b}}}}{1+b_{\mathrm{b}} P^{\nu_{\mathrm{b}}}} \quad (1)$$

where n is the absolute amount of gas adsorbed in mmol/g, $q_{\mathrm{sat,I}}$ are the saturation capacities in mmol/g, b_i are the Langmuir parameters in bar^{-1}, P is the gas pressure in bar, and v_i are the dimensionless Freundlich parameters for sites a and b. These parameters were determined using a least-squares fitting method, and are given in ESI Tables S1-S10.

Differential enthalpy

The differential enthalpy of adsorption for each gas was extracted from the temperature dependence of the isotherms using the Clausius–Clapyron relationship.[60] The adsorption isotherm fits were numerically inverted and solved as $P(n)$. The differential enthalpy, h, can then be determined at a constant loading using eqn 2:

$$h = -R\, d(lnP)/d(1/T) \quad (2)$$

where R is the ideal gas constant, P is the pressure at a given loading, and T is the data collection temperature (298.15, 308.15, or 318.15 K).

Ideal Adsorbed Solution Theory

Single-component equilibrium adsorption isotherm data can be employed to simulate adsorbed-phase compositions in the presence of gases containing multiple species, using Ideal Adsorbed Solution Theory (IAST). [61,62,63] In the simplest case, binary selectivities can be calculated as the ratio of the adsorbed phase mole fractions relative to the ratio of gas phase mole fractions of two components, given by eqn 3:

$$S = (x_1 / x_2)/(y_1 / y_2) \quad (3)$$

where S is the ideal selectivity for component 1 over component 2, x is the adsorbed phase mole fraction, and y is the gas phase mole fraction. This theory can also be extended to multicomponent mixtures to predict equilibrium compositions under a given OCM mixture, which is discussed in the ESI.

Transient breakthrough experiments

Breakthrough experiments were performed using a custom-built apparatus constructed of primarily 1/8" copper tubing fitted with Swagelok fittings and valves to control the flow of the gas either through the sample holder or to bypass the sample holder and flow directly to a gas chromatograph (GC) used to monitor outflow composition. Cylinders of premixed 1:1 ethane:ethylene, CO_2, and CH_4 were attached to the breakthrough manifold via MRS mass flow controllers to control gas flow. The Mn_2(*m*-dobdc) sample was pelletized using a 5mm evacuatable pellet die and broken into pieces using a 20-40 mesh sieve, and ~0.555 g of sample was then loaded into one vertical component (13.335 cm long, 0.4572 cm i.d.) of a U-shaped sample holder comprised of 1/4" tubing and fitted with Swagelok VCR fittings with fritted (0.5 μm) gaskets to prevent sample escaping from the bed. The U-

shaped tubing was immersed in a water bath and connected to the breakthrough manifold. The Mn_2(*m*-dobdc) sample was activated in the sample holder by heating it with heating tape at 180 °C under flowing He. The sample was then cooled to 25 °C for the breakthrough experiments using a total flow rate of 3–4 mL/min. Prior to flowing through the packed Mn_2(*m*-dobdc) sample, the gas mixture outflow was monitored using the GC to ensure the expected composition and separation. The mixture was then flowed through the packed bed of Mn_2(*m*-dobdc) and the outflow was recorded by the GC every 2 min for each gas mixture. The outflow composition was analyzed by gas chromatography using a SRI Instruments 8610V GC equipped with a 6' HayeSep D column, which was kept at 90 °C. The GC effluent was then fed into a flow meter to instantaneously monitor the volumetric flow rate of the gas through the column. The flow rate of each individual component was then calculated using eqn 4:

$$F_i(t) = y_i(t) * F^{\mathrm{tot}}(t) \qquad (4)$$

where $F_i(t)$ is the flow rate of species *i* at time *t* in mL/min, y_i is the fraction of component *i* measured from the peak areas in the gas chromatogram, and $F^{\mathrm{tot}}(t)$ is the instantaneous total flow rate of gas at the time the sample was injected into the GC, in mL/min. The quantity $F_i(t)/F_0$ is the flow of component *i* in the outlet stream relative to the total flow rate after breakthrough of all components.

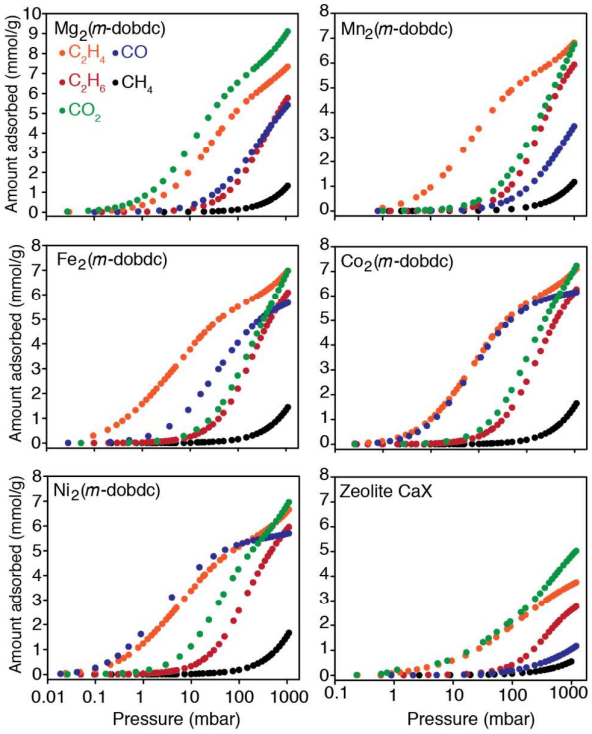

Fig. 2 Adsorption isotherms of ethylene, ethane, CO_2, CO, and CH_4 in M_2(*m*-dobdc) (M = Mg, Mn, Fe, Co, Ni) and in zeolite CaX at 25 °C.

In a given experiment, after all components had broken through the packed Mn_2(*m*-dobdc) bed, the flow was switched to He or another purge gas and the sample heated to 180 °C using heating tape to fully desorb adsorbed components from the column. All data were recorded and analyzed using PeakSimple software.

Breakthrough simulations

The Aspen Adsorption simulation platform was used to model the adsorbent bed system, which enables understanding of adsorption profiles across the bed (the mass transfer zone), assessment of the working capacity of the material, and predictions of the material performance in process cycles.

The modelling was performed in three steps. First, the model bed properties (bed height, diameter, mass, particle radius) and process conditions (pressure, temperature, flow rate, gas composition) were chosen to match the experimental setup. Experimentally-obtained single-component adsorption isotherms were used as the thermodynamic equilibrium model, while mass transfer coefficients for each component were maintained as independent variables that were adjusted to match the simulated and experimentally-measured single-component breakthrough curves (ESI, Figs. S1-S7). Second, the mass transfer coefficients obtained from fitting the experimental breakthrough curves were validated by comparison with dual-component experimental breakthrough curves (ESI, Fig. S8). Finally, the validated simulation model was used to predict the performance of the material with a typical OCM gas effluent mixture. The model configuration and key equations are specified in the ESI.

Results and discussion

Gas adsorption isotherms

Temperature-dependent equilibrium gas adsorption measurements can reveal a great deal of information about how a molecule interacts with an adsorbent. In the case of the raw data for ethylene, ethane, CO, CO_2, and methane adsorption in M_2(*m*-dobdc), it is possible to gauge relative binding strength and the adsorption capacity for each gas (Fig. 2). The differential enthalpies for adsorption for each of these gases are shown in Fig. 3 and compared across a constant loading of 0.5 mmol/g. For M_2(*m*-dobdc), the principle interaction with all adsorbates is electrostatic, in which the metal sites act as exposed cationic charges that can polarize proximal gas molecules. As such, all of these materials bind the highly-polarizable ethylene with binding enthalpies ranging from –44.1 ± 1.2 for Mg_2(*m*-dobdc) to –52.8 ± 1.0 kJ/mol for Fe_2(*m*-dobdc). This electrostatic interaction is well-illustrated by the previously reported single crystal X-ray diffraction structure of ethylene bound to Co_2(*m*-dobdc), which reveals a side-on binding interaction with metal–carbon distances of 2.743 Å and 2.667 Å.[53] However, a combination of cationic charge density, ionic radius, and π-back donation character will all subtly influence the binding of ethylene relative to the other gases in this study. As will be outlined further below, both Mn_2(*m*-dobdc) and Fe_2(*m*-dobdc) possess the ideal

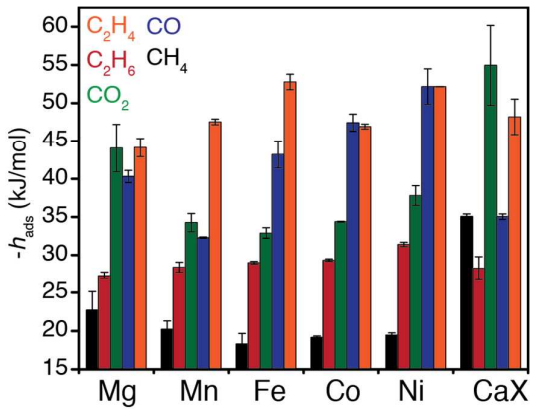

Fig. 3 Differential enthalpies of adsorption of CH_4, C_2H_6, CO_2, CO, and C_2H_4, in M_2(*m*-dobdc) (M = Mg, Mn, Fe, Co, Ni) and zeolite CaX. Enthalpies were calculated at a constant loading of 0.5 mmol/g in each adsorbent.

combination of these properties to display highly selective ethylene adsorption over the other measured gases.

The binding of H_2 in M_2(*m*-dobdc) materials has been thoroughly investigated under both sub-ambient and elevated pressures for H_2 storage.[64] Under the partial pressures of interest for an OCM effluent gas separation, the isosteric heat of H_2 adsorption is on the order of –10 to –12.5 kJ/mol, and thus this molecule cannot compete for adsorption sites with the other, much more strongly interacting species in the mixture.[59]

Among the frameworks, methane adsorbs most strongly in Mg_2(*m*-dobdc), with a binding enthalpy of –22.7 ± 2.4 kJ/mol. However, zeolite CaX has significantly stronger interactions with CH_4 overall, and the methane adsorption enthalpy in this material is –35.0 ± 0.4 kJ/mol. These relative magnitudes coincide with the fact that Mg^{2+} is the most electropositive cation within the metal–organic framework series while Ca^{2+} in CaX is the most electropositive cation overall. The relative electropositivity of the binding sites in Mg_2(*m*-dobdc) and CaX is even more apparent upon considering the isosteric heats for CO_2 adsorption in these materials, which are –44.0 ± 3.1 and –54.9 ± 5.2 kJ/mol, respectively. These values are substantially larger than those measured for CO_2 binding in the transition metal frameworks, and thus these two materials would not be capable of selecting for ethylene over CO_2 out of the OCM reaction effluent mixture.

While the electropositivity of the M^{2+} centers is the dominant factor influencing CH_4 and CO_2 adsorption in M_2(*m*-dobdc) and CaX, the trends in adsorption and binding enthalpy observed for CO are better understood by invoking an interplay of metal cationic charge density and some slight π-back donation ability. Carbon monoxide binds most strongly in Ni_2(*m*-dobdc) and Co_2(*m*-dobdc), with adsorption enthalpies of –52.0 ± 4.8 and –47.4 ± 1.1 kJ/mol, respectively, followed by the Fe, Mg, and Mn frameworks. This trend also matches that characterized previously for CO binding in the isomeric M_2(dobdc) (M = Mg, Mn, Fe, Co, Ni, Zn; $dobdc^{4-}$ = 2,5-dioxido-1,4-benzenedicarboxylate) frameworks,[65] including through the use of *in-situ* gas dosing during neutron diffraction and FT-IR experiments. The infrared spectra reveal that upon adsorption of CO to the divalent metal cation, the C-O stretching frequency is blue-shifted, consistent with non-classical metal-CO interactions.[44] Given their strong interaction with CO, Co_2(*m*-dobdc) and Ni_2(*m*-dobdc) are poorly suited for selectively separating ethylene from the OCM effluent mixture.

In contrast to the other materials, Mn_2(*m*-dobdc) and Fe_2(*m*-dobdc) do not exhibit an exceptionally strong affinity for CH_4, CO_2, or CO, and they show the greatest relative affinity for ethylene. Accordingly, these two frameworks were further evaluated for their ethylene separation performance under more realistic conditions. Finally, relative to other materials, Mn_2(*m*-dobdc) and Fe_2(*m*-dobdc) exhibit significantly higher ethylene adsorption capacity at the relevant partial pressure. For an ethylene partial pressure of 400 mbar at a temperature of 25 ˚C, the capacities of Mn_2(*m*-dobdc) and Fe_2(*m*-dobdc) are 6.12 and 6.19 mmol/g, respectively. These are substantially higher than in Ag-exchanged zeolite A (2.2 mmol/g) or zeolite ITQ-55 (1.3 mmol/g).[66,67]

Ideal selectivities

Binary selectivities for ethylene and each additional major species in the OCM effluent were calculated by fitting the equilibrium gas adsorption isotherms with a dual-site Langmuir-Freundlich equation and applying the Ideal Adsorbed Solution Theory (IAST) model.[61-63] The resulting selectivities at

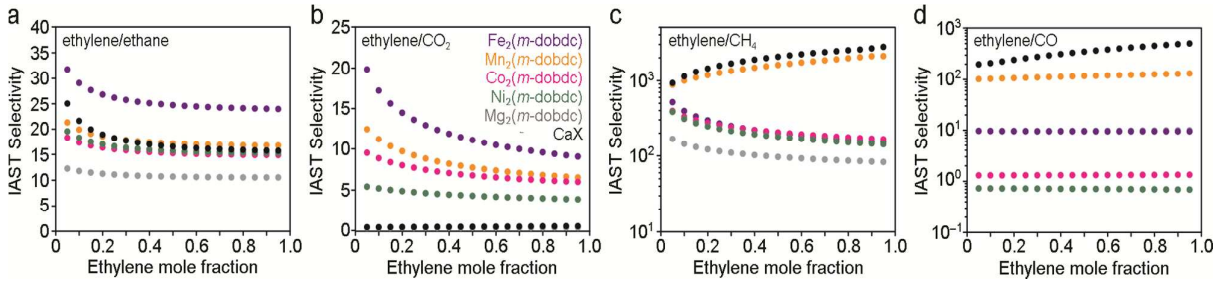

Fig. 4 Selectivities for ethylene over other gases in the OCM effluent mixture as calculated by the ideal adsorbed solution theory. The IAST selectivities for (a) ethylene/ethane, (b) ethylene/CO_2, (c) ethylene/CH_4, and (d) ethylene/CO were determined for M_2(*m*-dobdc) (M = Mg, Mn, Fe, Co, Ni) and zeolite CaX.

25 ˚C are plotted in Fig. 4 as a function of ethylene mole fraction in the gas phase relative to the competing species, since the selectivity will be dependent on the OCM gas composition. The ethylene/ethane ratio in the OCM reaction effluent is ~1.25:1. At this value, Fe_2(*m*-dobdc) shows the highest selectivity of 24.6 at 25 °C, followed by Mn_2(*m*-dobdc) with a selectivity of 17.0 (Fig 4a). Notably, these selectivities are much higher than any measured thus far for other adsorbents that utilize a rapid, reversible, and physisorptive mechanism.[53] A similar trend exists for the ethylene/CO_2 selectivities at an ethylene mole fraction of 0.5, reflecting the ~1:1 ethylene:CO_2 ratio present in the OCM reaction effluent. Notably, Fe_2(*m*-dobdc) displays the highest selectivity of 11.0, followed by Mn_2(*m*-dobdc) with a selectivity of 7.7. In contrast, both Mg_2(*m*-dobdc) and zeolite CaX exhibit near-zero ethylene/CO_2 selectivity, as expected from the adsorption enthalpies. In agreement with the adsorption isotherms and differential enthalpies of adsorption, all frameworks are highly selective for ethylene over CH_4, binding only one molecule of CH_4 for every 1000 or more ethylene molecules adsorbed.

This series of adsorbents varies most in their ability to separate ethylene from CO. For example, Ni_2(*m*-dobdc) binds CO with a selectively over ethylene that is orders of magnitude greater than that exhibited by the other frameworks and CaX. As such, CO would remain a substantial component of the OCM effluent if the Ni framework were used in a purification process—a detrimental result if the ethylene is to be used later for polymerization. While Fe_2(*m*-dobdc) exhibits the highest ethylene/ethane selectivity across the series, it displays only a modest ethylene/CO selectivity of ~10 compared to that of Mn_2(*m*-dobdc), which is an order of magnitude higher at 125 for a 3:1 mixture of ethylene:CO. The Fe compound is also significantly less stable in air than the other frameworks, and therefore based on equilibrium adsorption and thermodynamic analysis, Mn_2(*m*-dobdc) is clearly the best material out of those examined here for the purification of the OCM effluent.

Beyond binary IAST calculations, the theory can be extended to include a more complex mixture of gases. Similar to a distillation, the composition of the mixture can be determined under a series of equilibrium stages, wherein the adsorbed phase at one stage is used as a feed to the subsequent stage (ESI, Fig. S11). Through this type of simulation, we found that only three theoretical equilibrium stages would be necessary to obtain a 99.9% ethylene product using Mn_2(*m*-dobdc) as the adsorbent and starting with the OCM effluent composition as the initial feed (Fig. 1). When compared with conventional cryogenic distillation, which utilizes more than 50 stages for ethylene/ethane separation alone, it is clear that an optimized adsorption process can vastly improve the outcome of a purification process.[1]

Transient breakthrough experiments and simulations

Transient breakthrough experiments were conducted on Mn_2(*m*-dobdc) to examine the performance of this material under more realistic process conditions. Under a single-component gas flow, Mn_2(*m*-dobdc) exhibits breakthrough

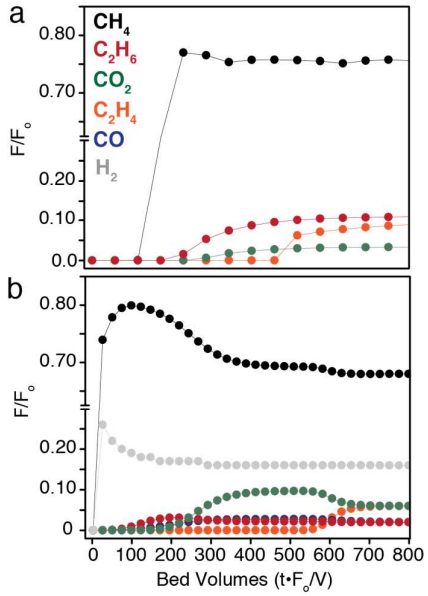

Fig. 5 (a) Experimental breakthrough curves for a simplified OCM gas mixture at 25 °C and a total pressure of 6.2 bar. (b) Transient breakthrough curves for a simulated mixture of OCM effluent gases at the same total pressure and temperature. Mass transfer coefficients for ethylene, ethane, CO_2 and CH_4 were found to be 0.0125 s^{-1}, 0.0037 s^{-1}, 0.01 s^{-1}, and 0.004 s^{-1}.

capacities of 6.8, 6.3, 4.7, and 0.1 mmol/g for ethylene, ethane, CO_2, and CH_4, respectively (Figs. S1–S4). These values are in good agreement with the equilibrium adsorption measurements, indicating that gas transport is relatively rapid. Slight differences in the adsorptive capacities determined from breakthrough experiments and equilibrium measurements are likely the result of non-isothermal adsorption, associated with a large exothermic release during gas adsorption that increases the temperature of the bed during measurement.

The single component breakthrough curves were used in conjunction with equilibrium adsorption data to determine mass transfer coefficients (Table S7). Interestingly, the mass transfer coefficients are most closely correlated with the adsorption enthalpy of a particular gas, as opposed to physical characteristics such as molecular weight. For example, methane has a smaller kinetic diameter and lower mass than ethylene, and thus gas-phase and mesopore diffusion of methane is expected to be faster than that of ethylene. However, the mass transfer coefficients for ethylene and methane were found to be 0.0125 and 0.004 s^{-1}, respectively, indicating that diffusion within the metal–organic framework pores may be the dominating factor determining the kinetics, wherein a steeper concentration gradient exists for more strongly adsorbing gases.

Along with equilibrium adsorption data, these mass flow coefficients were used in an Aspen adsorption model to evaluate the performance of Mn_2(*m*-dobdc) in the separation of ethylene and ethane, and were validated by their ability to reproduce binary breakthrough curves (Fig. S8). Under a flowing equimolar mixture of ethylene and ethane, steep

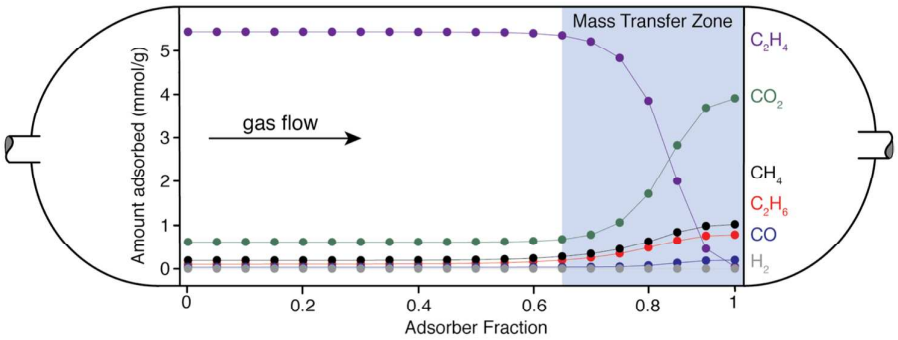

Fig. 6 Snapshot of the simulated adsorbent bed composition profile following bed saturation with a representative oxidative coupling of methane effluent mixture. The composition is profiled given ethylene recovery threshold of 100 ppm ethylene at the outlet. The mass transfer zone indicates the portion of the column that is under non-equilibrium conditions. Upstream of the mass transfer zone is under equilibrium conditions.

breakthrough of ethane occurs first, followed by ethylene (Fig. S10). These sharp breakthrough curves suggest that the mass transfer zone is small relative to the size of the bed, implying that the majority of the bed is useful in conducting the separation. The experiment was repeated with a mixture of ethylene, ethane, and CO_2, resulting in a breakthrough pattern in which ethane was once again observed first, followed by CO_2, and finally ethylene (Fig. S11). The breakthrough curves of each gas remain steep, indicating retention of fast adsorption kinetics.

Upon testing a mixture of ethylene, ethane, CH_4, and CO_2 at a total pressure of 6.2 bar (representing partial pressures of 0.45, 0.45, 0.65, and 4.65 bar for ethylene, ethane, CO_2 and CH_4, respectively), a clean separation of ethylene was again observed. Consistent with the equilibrium adsorption isotherms, differential enthalpy trends, IAST calculations, and pure-component breakthrough measurements, CH_4 breaks through first, followed by ethane, CO_2, and finally ethylene (Fig. 5a). Using the same adsorbent conditions, a more complex gas mixture including CO and H_2 was modelled using Aspen Adsorption, representing a total of six components and a total pressure of 7 bar (partial pressures of 0.42, 0.14, 4.75, 0.14, 0.42, and 1.12 bar for ethylene, ethane, CH_4, CO, CO_2, and H_2, respectively). In this model, the same mass transfer coefficient was used for CO as was measured for ethylene, a good approximation given the similar kinetic diameters of these two gases. The results of the simulation show CH_4 and H_2 to break through rapidly, followed by CO, ethane, CO_2, and finally ethylene (Fig. 5b).

Finally, we determined a realistic capacity for an adsorption process using Mn_2(*m*-dobdc) by elucidating the transient concentration profile of a cylindrical bed over the course of an adsorption simulation. In this analysis, as in all adsorption processes, there is an inherent trade-off between material capacity and recovery of the desired adsorbate, due to the existence of a mass transfer zone. Accordingly, for an ethylene breakthrough concentration of 100 ppm (Fig. 6), a snapshot of a transient bed profile revealed a bed utilization factor of 82%, while for an ethylene breakthrough concentration of 1000 ppm (Fig. S13) the bed utilization factor increases to 86%.

All together, the experimental and simulated transient breakthrough experiments demonstrate the exceptional ability of Mn_2(*m*-dobdc) to purify ethylene from a simulated OCM effluent mixture. Significantly, this is the first adsorbent reported to cleanly separate ethylene from this complex mixture of gases.

Conclusions

The use of methane as an alternative feedstock for ethylene production via the oxidative coupling of methane represents a promising energy- and cost-effective alternative to the derivation of ethylene from fossil fuels. However, implementation of this process on a large-scale is hindered by the co-production of a complex mixture of other gases including ethane, CO_2, CO, and CH_4, which are prohibitively challenging to separate from ethylene using a conventional distillation approach. We have evaluated the M_2(*m*-dobdc) family of frameworks (with M = Mg, Mn, Fe, Co, and Ni) as candidate materials for the separation of ethylene in an adsorbent-based process, and compared their performance to that of the commercial adsorbent zeolite CaX. A suite of adsorption data as well as experimental and simulated breakthrough results indicate that Mn_2(*m*-dobdc)—which displays a high selectivity for ethylene over CO_2, CO, and CH_4, large ethylene capacities, and fast adsorption kinetics—is the most promising out of these materials for the separation of ethylene from the oxidative coupling of methane effluent mixture. In addition to identifying Mn_2(*m*-dobdc) as an outstanding adsorbent for separating ethylene from this specific mixture, our data suggest that Mg_2(*m*-dobdc) may be useful as an adsorbent that can co-capture ethylene and CO_2, while Ni_2(*m*-dobdc) or Co_2(*m*-dobdc) may be used effectively for processing effluent streams where CO is absent or where it is desirable to isolate both ethylene and CO. These results show that metal–organic framework adsorbents can be used to dramatically improve the efficiency of the OCM effluent separation, potentially supporting the large-scale deployment

of this ethylene production process and offering a competitive alternative to the decades-old fossil-based ethylene production routes.

Conflicts of interests

The authors declare the following competing financial interests: J.R.L. has a financial interest in Mosaic Materials, Inc., a start-up company working to commercialize metal–organic frameworks, including the M_2(*m*-dobdc) materials investigated here for gas separations. The University of California, Berkeley has filed a patent on these materials, on which M.T.K. and J.R.L. are included as inventors.

Acknowledgements

We gratefully acknowledge Siluria Technologies for financial support of this research. This material is based upon work supported by the Department of Energy, Office of Energy Efficiency and Renewable Energy (EERE), under Award Number DE-EE0005769. Additionally, we would like to thank Dr. Aihua Zhang, Dr. Greg Nyce, Dr. Fabio Zurcher, Dr. Joel Cizeron, and Dr. Kurtis Knapp of Siluria Technologies for helpful discussions relating to the application of adsorbents in the OCM process, Dr. Katie Meihaus of the University of California, Berkeley for editorial assistance, and the National Science Foundation for fellowship support of M.T.K.

Notes and references

1. R. B. Eldridge, *Ind. Eng. Chem. Res.* 1993, **32**, 2208-2212.
2. B. L. Farrell, V. O. Igenegbai, S. Linic, *ACS Catal.* 2016, **6**, 4340-4346.
3. B. L. Farrell, S. Linic, *Catal. Sci. Technol.* 2016, **6**, 4370-4376.
4. E. V. Kondratenko, M. Baerns, *Handbook of Heterogeneous Catalysis;* Wiley-VCH, 2008.
5. G. E. Keller, M. M. Bhasin, *J. Catal.* 1982, **73**, 9-19.
6. K. Otsuka, K. Jinno, A. J. Morikawa, *Catal.* 1986, **100**, 353-359.
7. L. Mleczko, M. Baerns, *Fuel. Proc. Tech.* 1995, **42**, 217-248.
8. J. H. Lunsford, *Catal. Today* 1990, **6**, 235-259.
9. J. H. Lundsford, *Catal. Today* 2000, **2**, 165-174.
10. J. A. Sofranko, J. J. Leonard, A. J. Jones, *Catal.* 1987, **103**, 302-310.
11. J. E. Elshof, H. J. M. Bouwmeester, H. Verweij, *Appl. Catal. A.* 1995, **130**, 195-212.
12. T. Nishiyama, K.-I. Aika, *J. Catal.* 1990, **122**, 346-351.
13. B. Beck, V. Fleischer, S. Arndt, M. G. Hevia, A. Urakawa, P. Hugo, R. Schomacker, *Catal. Today*, 2014, **228**, 212-218.
14. S. Bhatia, C. Y. Thien, A. R. Mohamed, *Chem Eng. J.* 2009, **148**, 525-532.
15. Y. S. Su, J. Y. Ying, W. H. Green, *J. Catal.* 2003, **218**, 321-333.
16. D. M. McCann, D. Lesthaeghe, P. W. Kletnieks, D. R. Guenther, M. J. Mayman, V. V. Speybroeck, M. Waroquier, J. F. Haw, *Agnew. Chemie* 2008, **120**, 5257-5260.
17. B. P. C. Hereijgers, F. Bleken, M. H. Nilsen, S. Svelle, K.-P Lillerud, M. Bjorgen, B. M. Weckhuysen, U. Olsbye, *Catal.* 2009, **264**, 77-87.
18. F. Blaken, M. Bjorgen, L. Palumbo, S. Bordiga, S. Svelle, K.-P. Lillerud, U. Olsbye, *Top. Catal.* 2009, **52**, 218-228.
19. D. R. Dubois, D. L. Obrzut, J. Liu, J. Thudimadathil, P. M. Adekkanattu, J. A. Guin, A. Punnoose, M. S. Seehra, *Fuel Proc. Technol.* 2003, **83**, 203-218.
20. C. D. Chang, C. T.-W. Chu, R. F. Socha, *J. Catal.* 1984, *86*, 289-296.
21. P. Tian, Y. Wei, M. Ye, Z. Liu, *ACS Catal.* 2015, **5**, 1922-1938.
22. K. Feng, S. J. Davis, L. Sun, K. Hubacek, *Nat. Commun.* 2015, **6**, 7714.
23. I. M. Nasir, T. I. Gazhi, R. Omar, 2012, **12**, 258-269.
24. W. P. Barber, D.C. Stuckey, *Water Res.* 1999, **33**, 1559-1578.
25. U.S. Department of Agriculture. *Biogas Opportunities Roadmap. (2014).*
26. S. Lin, C. S. Diercks, Y. Zhang, N. Kornienko, E. M. Nichols, Y. Zhao, A. R. Paris, D. Kim, P. Yang, O. M. Yaghi, C. J. Chang, *Science* 2015, **346**, 1208-1213.
27. O. M. Yaghi, H. Li, M. Eddaoudi, M. O'Keefe, *Nature* 1999, **402**, 276–279.
28. S. Kitagawa, R. Kitaura, S.-I. Noro, Angew. Chem., Int. Ed. 2004, **43**, 2334–2375.
29. R. Matsuda, R. Kitaura, S. Kitagawa, Y. Kubota, R. V. Belosludov, T. C. Kobayashi, H. Sakamoto, T. Chiba, M. Takata, Y. Kawazoe, Y. Mita, Nature 2005, **436**, 238– 241.
30. A. R. Millward, O. M. Yaghi, J. Am. Chem. Soc. 2005, **127**, 17998–17999.
31. G. Ferey, Chem. Soc. Rev. 2008, **37**, 191–214.
32. A. U. Czaja, N. Trukhan, U. Müller, *Chem. Soc. Rev*. 2009, **38**, 1284–1293.
33. B. Chen, S. Xiang, G. Qian, Acc. *Chem. Res*. 2010, **43**, 1115−1124.
34. H.-C. Zhou, J. R. Long, O. M. Yaghi, *Chem. Rev*. 2012, **112**, 673−674.
35. J.-R. Li, J. Sculley, H.-C. Zhou, *Chem. Rev.* 2012, **112**, 869–932.
36. A. Schneemann, S. Henke, I. Schwedler, R. A. Fischer, *ChemPhysChem* 2014, **15**, 823–839.
37. A. O. Yazaydin, R. Q. Snurr, T.-H. Park, K. Koh, J. Liu, M. D. LeVan, A. I. Benin, P. Jakubczak, M. Lanuza, D. B. Galloway, J. J. Low, R. R. Willis, *J. Am. Chem. Soc.* 2009, **131**, 18198-18199.
38. A. O. Yazaydin, A. I. Benin, S. A. Faheem, P. Jakubczak, J. J. Low, R. R. Willis, R. Q. Snurr, *Chem. Mater.* 2009, **21**, 1425-1430.
39. S. R. Caskey, A. G. Wong-Foy, A. J. Matzger, *J. Am. Chem. Soc.* 2008, **130**, 10870−10871.
40. M. Dinca, J. R. Long, *Angew. Chem., Int. Ed.* 2008, **47**, 6766−6779.
41. P. D. C. Dietzel, V. Besikiotis, R. Blom, *J. Mater. Chem.* 2009, **19**, 7362−7370.
42. Z. R. Herm, J. A. Swisher, B. Smit, R. Krishna, J. R. Long, *J. Am. Chem. Soc.* 2011, **133**, 5664−5667.
43. J. A. Mason, K. Sumida, Z. R. Herm, R. Krishna, J. R. Long, *Energy Environ. Sci.* 2011, **4**, 3030−3040.
44. E. D. Bloch, L. M. Murray, W. L. Queen, S. Chavan, S. N. Maximoff, J. P. Bigi, R. Krishna, V. K. Peterson, F. Grandjean, G. J. Long, B. Smit, S. Bordiga, C. M. Brown, J. R. Long, *J. Am. Chem. Soc.* 2011, **133**, 14814−14822.
45. E. D. Bloch, W. L. Queen, R. Krishna, J. M. Zadrozny, C. M. Brown, J. R. Long, *Science* 2012, **335**, 1606−1610.
46. S. J. Geier, J. A. Mason, E. D. Bloch, W. L. Queen, M. R. Hudson, C. M. Brown, J. R. Long, *Chem. Sci.* 2013, **4**, 2054−2061.
47. K. Sumida, D. R. Rogow, J. A. Mason, T. M. McDonald, E. D. Bloch, Z. R. Herm, T.-H. Bae, J. R. Long, *Chem. Rev.* 2012, **112**, 724− 781.
48. Z. R. Herm, R. Krishna, J. R. Long, *Microporous Mesoporous Mater.* 2012, **151**, 481−487.

49. Y. Peng, V. Krungleviciute, I. Eryazici, J. T. Hupp, O. K. Farha, T. Yildirim, *J. Am. Chem. Soc.* 2013, **135**, 11887−11894.
50. J. A. Mason, M. Veenstra, J. R. Long, *Chem. Sci.* 2014, **5**, 32−51.
51. Z. R. Herm, E. D. Bloch, J. R. Long, *Chem. Mater.* 2014, **26**, 323−338.
52. X. Duan, Y. He, Y. Cui, Y. Yang, R. Krishna, B. Chen, G. Qian, *RSC Adv.* 2014, **4**, 23058−23063.
53. J. E. Bachman, M. T. Kapelewski, D. A. Reed, M. I. Gonzalez, J. R. Long, *J. Am. Chem. Soc.* 2017, **139**, 15363.
54. T. M. McDonald, J. A. Mason, X. Kong, E. D. Bloch, D. Gygi, A. Dani, V. Crocella, F. Giordanino, S. O. Odoh, W. Drisdell, B. Vlaisavljevich, A. L. Dzubak, R. Poloni, S. K. Schnell, N. Planas, K. Lee, T. Pascal, L. F. Wan, D. Prendergast, J. B. Neaton, B. Smit, J. B. Kortright, L. Gagliardi, S. Bordiga, J. A. Reimer, J. R. Long, *Nature*, 2015, **519**, 303-311.
55. D. A. Reed, D. J. Xiao, M. I. Gonzalez, L. E. Darago, Z. R. Herm, F. Grandjean, J. R. Long, J. Am. Chem. Soc. 2016, **138**, 5594-5602.
56. Z. R. Herm, B. M. Wiers, J. A. Mason, J. M. van Baten, M. R. Hudson, P. Zajdel, C. M. Brown, N. Masciocchi, R. Krishna, J. R. Long, *Science*, 2013, **340**, 960-964.
57. S. Hosseinpour, S. Fatemi, Y. Mortazavi, M. Gholamhoseini, M. T. Ravanchi, *Sep. Sci. Technol*. 2010, **46**, 349-355.
58. Y. Li, H. Yi, X. Tang, F. Li, Q. Yuan, *Chem. Eng. J.* 2013, *229*, 50-56.
59. M. T. Kapelewski, S. J. Geier, M. R. Hudson, D. Stuck, J. A. Mason, J. N. Nelson, D. J. Xiao, Z. Hulvey, E. Gilmour, S. A. FitzGerald, M. Head-Gordon, C. M. Brown, J. R. Long, *J. Am. Chem. Soc.* 2015, **136**, 12119-12129.
60. W. Rudzinski, D. H. Everett, *Adsorption of Gases on Heterogeneous Surfaces*; Academic Press, Inc: CA, 1992.
61. A. L. Myers, J. M. Prausnitz, J. M. *AIChE Journal* 1965, **11**, 121-127.
62. M. D. LeVan, T. Vermeulen, *J. Phys. Chem.* 1981, **85**, 3247-3250.
63. E. Richter, S. Wilfried, A. L. Myers, *Chem. Eng. Sci.* 1989, **44**, 1609-1616.
64. M. T. Kapelewski, T. Runčevski, J. D. Tarver, H. Z. H. Jiang, K. E. Hurst, P. A. Parilla, A. Ayala, T. Gennett, S. A. FitzGerald, C. M. Brown and J. R. Long, *Submitted.*
65. E. D. Bloch, M. R. Hudson, J. A. Mason, S. Chavan, V. Crocella, J. D. Howe, K. Lee, A. L. Dzubak, W. L. Queen, J. M. Zadrozny, S. J. Geier, L.-C. Lin, L. Gagliardi, B. Smit, J. B. Neaton, S. Bordiga, C. M. Brown, J. R. Long, *J. Am. Chem. Soc*. 2014, *136*, 10752−10761.
66. S. Aguado, G. Bergeret, C. Daniel, D. Farrusseng, *J. Am. Chem. Soc.* 2012, **134**, 14635-14637.
67. P. J. Bereciartua, A. Cantín, A. Corma, J. L. Jordá, M. Palomino, F. Rey, S. Valencia, E. W. Corcoran, P. Kortunov, P. I. Ravikovitch, A. Burton, C. Yoon, Y. Wang, C. Paur, J. Guzman, A. R. Bishop, G. L. Casty, *Science* 2017, **358**, 1068-1071.

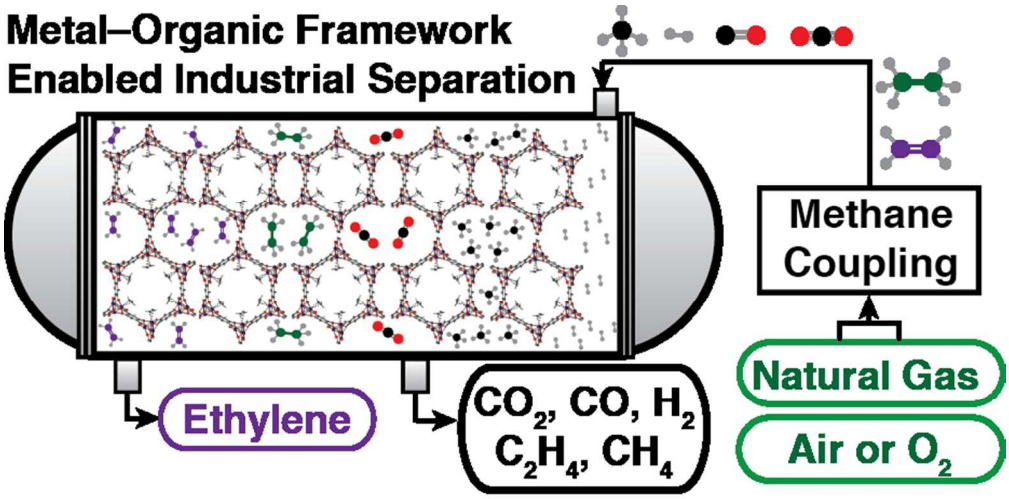
Metal–Organic Framework
Enabled Industrial Separation
Methane
Coupling
Natural Gas
Air or O_2
Ethylene
CO_2, CO, H_2
C_2H_4, CH_4